Vol 18 No 12, December 2009
1674-1056/2009/18(12)/5354-08

Chinese Physics B

© 2009 Chin. Phys. Soc.
and IOP Publishing Ltd

# Four-wave mixing and six-wave mixing in a four-level confined atomic system*

Li Chang-Biao(李昌彪), Zhang Yan-Peng(张彦鹏)†, Nie Zhi-Qiang(聂志强), Zheng Huai-Bin(郑淮斌), Shi Mei-Zhen(史美震), Liu Dong-Ning(刘东宁), Song Jian-Ping(宋建平), and Lu Ke-Qing(卢克清)

*Key Laboratory for Physical Electronics and Devices of the Ministry of Education & Shaanxi Key Laboratory of Information Photonic Technique, Xi'an Jiaotong University, Xi'an* 710049, *China*

(Received 13 April 2009; revised manuscript received 24 May 2009)

We have investigated coexisting four-wave mixing and six-wave mixing (SWM) in ultra-thin, micrometre and long vapour cells. There exists competition between Dicke-narrowing features and polarization interference in the micrometre cell. The oscillation behaviour of SWM signal intensities and linewidths results from destructive interference. With a larger destructive interference, the SWM signal in ultra-thin cells shows a narrow spectrum, in contrast to the long cell case. Due to the Dicke-narrowing features, a narrow spectrum can be obtained, and such spectra can be used for high precision measurements and metrological standards.

**Keywords:** Dicke-narrowing features, polarization interference, multi-wave mixing
**PACC:** 4265, 3280

## 1. Introduction

High-resolution spectroscopy of atoms confined in an ultra-thin cell is a promising tool for the investigation of complex spectra of atoms and molecules.[1] Recently, electromagnetically induced transparency (EIT) has led to the observation of dark resonances in free space,[2−4] micrometric cells,[5] and even in ultra-thin cells.[6] In addition, Ai *et al* [7] have observed a significantly enhanced degenerate four-wave mixing (FWM) signal at noncycling transitions in a thin cell.[7] Later on, enhanced FWM processes due to atomic coherence were experimentally demonstrated in a four-level system.[8,9] Efficient six-wave mixing (SWM) has also been observed in a four-level close-cycled N-type rubidium atomic system.[10] In the previous experimentally studied close-cycled system, FWM and SWM processes could not coexist in a given configuration and different order nonlinearities could only be observed individually. In our recent studies, we demonstrated that third-order and fifth-order nonlinear processes can coexist in open atomic systems. In terms of amplitude, coexisting SWM processes can become comparable or even greater than the companion FWM processes by manipulating the atomic coherence and multi-photon interferences between different energy levels in the systems.[11]

Compared with previous works, we find that some features are different from the previous ones and several advantages are present in this paper. Firstly, we present coexisting FWM and SWM in ultra-thin, micrometre and long cells, which are good systems for studying the interplay between nonlinear optical processes of different orders. Secondly, Dicke-narrowing features [7,12] are dominant in ultra-thin cells, while polarization interference[13] is dominant in long cells, and there exists competition between Dicke-narrowing features and polarization interference in micrometre cells. Thirdly, the oscillation behaviour of SWM signal intensities and linewidths results from destructive interference in the thin cell. When strong destructive interference occurs in an ultra-thin cell, the SWM signal shows a narrow spectrum. The purpose of this paper is to theoretically analyse the main spectroscopic feature of FWM and SWM in ultra-thin, micrometre and long cells. We put an emphasis on the study of line shape, intensity, AT splitting, suppression and enhancement of the FWM and SWM signals.

*Project supported by the National Natural Science Foundation of China (Grant No 60678005), the Foundation for the Author of National Excellent Doctoral Dissertation of China (Grant No 200339), the Fok Ying-Tong Education Foundation for Young Teachers in the Institutions of Higher Education of China (Grant No 101061), NCET-08-0431.
†Corresponding author. E-mail: ypzhang@mail.xjtu.edu.cn

## 2. Basic theory

Consider a five-level confined atomic system with four laser beams as shown in Fig.1(a). Three energy levels ($|0\rangle - |1\rangle - |2\rangle$) form a ladder type system when the pump beam $E_3$ ($\omega_3$, $\boldsymbol{k}_3$, $G_3$) is blocked. Simultaneously the probe beam ($E_1(\omega_1, \boldsymbol{k}_1, G_1)$) together with one of the pump beams ($E_2(\omega_2, \boldsymbol{k}_2, G_2)$ or $E_2'(\omega_2, \boldsymbol{k}_2', G_2')$) is shown as an EIT window, since the probe beam $E_1$ and the pump beam $E_2$ are in the two-photon Doppler-free (first-order) configuration (counter-propagating). When both beams $E_2$ and $E_2'$ are tuned on, an efficent FWM process can be generated to produce a conjugate signal at frequency $\omega_1$. The generated FWM signal propagates in the $\boldsymbol{k}_f = \boldsymbol{k}_1 + \boldsymbol{k}_2 - \boldsymbol{k}_2'$ direction due to the phase-matching condition, via the perturbation chain (F1) ($\rho_{00}^{(0)} \xrightarrow{\omega_1} \rho_{10}^{(1)} \xrightarrow{\omega_2} \rho_{20}^{(2)} \xrightarrow{-\omega_2} \rho_{10}^{(3)}$). By adding another energy level $|3\rangle$ and another laser field $E_3$ for level $|3\rangle$, the original energy level $|2\rangle$ will be dressed to produce two dressed states. Such a four-level system with a dressing field will modify the original FWM process (called singly dressed FWM) and generate SWM signals ($\boldsymbol{k}_s = \boldsymbol{k}_1 + \boldsymbol{k}_2 - \boldsymbol{k}_2' + \boldsymbol{k}_3 - \boldsymbol{k}_3$ via the SWM perturbation chain (S1) $\rho_{00}^{(0)} \xrightarrow{\omega_1} \rho_{10}^{(1)} \xrightarrow{\omega_2} \rho_{20}^{(2)} \xrightarrow{-\omega_3} \rho_{30}^{(3)} \xrightarrow{\omega_3} \rho_{20}^{(4)} \xrightarrow{-\omega_2} \rho_{10}^{(5)}$).

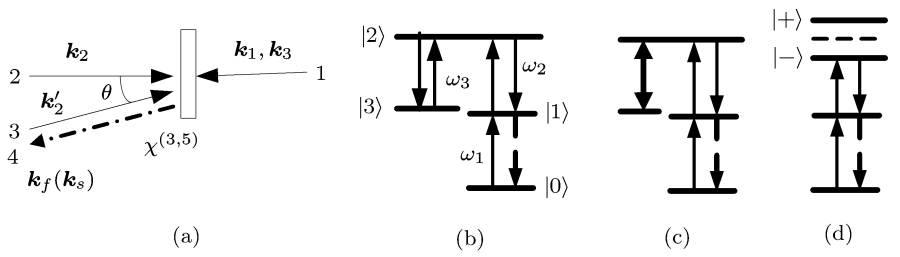



**Fig.1.** (a) Phase-conjugation geometry. (b) Energy-level diagram of the four-level confined atomic system. (c) Energy-level diagram for singly dressed four-wave mixing (DFWM). (d) Dressed-state picture.

In the SWM perturbation chain (S1), the subchain "$\rho_{20}^{(2)} \xrightarrow{-\omega_3} \rho_{30}^{(3)} \xrightarrow{\omega_3} \rho_{20}^{(4)}$" of the dressing field $E_3$ takes the place of $\rho_{20}^{(2)}$ in the chain F1. So we can modify the FWM chain as a singly dressed FWM chain (F2) $\rho_{00}^{(0)} \xrightarrow{\omega_1} \rho_{10}^{(1)} \xrightarrow{\omega_2} \rho_{(G_3\pm)0}^{(2)} \xrightarrow{-\omega_2} \rho_{10}^{(3)}$, where the subscript "2" of $\rho_{20}^{(2)}$ is replaced by "$G_3\pm$". This means that the dressing field $E_3$ influences the coherence $\rho_{20}^{(2)}$ of the FWM process and creates dressed states $|G_3\pm\rangle$ from level $|2\rangle$. According to this subchain, we can obtain coupling equations: $\dot{\rho}_{20}^{(2)} = -\Lambda_{20}\rho_{20}^{(r)} - \mathrm{i}\,G_3\rho_{30} + \mathrm{i}\,G_2^*\rho_{10}^{(1)}$, $\dot{\rho}_{30} = -\Lambda_{30}\rho_{30} + \mathrm{i}\,G_3\rho_{20}^{(2)}$ (here we consider all the matrix elements in the subchain "$\rho_{20}^{(2)} \xrightarrow{-\omega_3} \rho_{30}^{(3)} \xrightarrow{\omega_3} \rho_{20}^{(4)}$" and the connected matrix elements ($\rho_{20}^{(2)}$ and $\rho_{10}^{(3)}$) in the chain (F2)), and obtain $\mathrm{L}\{\rho_{20}^{(2)}\} = \mathrm{i}\,G_2'(s+\Lambda_{30})/[(s+\Lambda_{20})(s+\Lambda_{30})+G_3^2]$ from the coupling equation for $E_3$ interaction terms. Here L is the Laplace transform operator defined as $\mathrm{L}\{f(t)\} = \int_0^\infty f(t)\mathrm{e}^{-st}\mathrm{d}t$; the Doppler-shifted detunings are defined as $\Lambda_{20} = \Gamma_{20} + \mathrm{i}[\Delta_1 + \Delta_2 - k_1(1-\xi_2)v]$, $\Lambda_{30} = \Gamma_{30} + \mathrm{i}[\Delta_1 + \Delta_2 - \Delta_3 - k_1(1-\xi_2-\xi_3)v]$, where $\xi_2 = k_2/k_1$, $\xi_3 = k_3/k_1$, and $\Gamma_{ij} = \Gamma_{ji} = (\Gamma_i + \Gamma_j)/2$ represents the decay rate from level $|i\rangle$ to $|j\rangle$ ($i, j = 0, 1, 2, 3, i \neq j$). $\mathrm{L}\{\rho_{10}^{(1)}\} = \mathrm{i}\,G_1/[s(s+\Lambda_{10})]$ and $L\{\rho_{10}^{(3)}\} = \mathrm{i}\,G_2\mathrm{L}\{\rho_{20}^{(2)}\}/(s+\Lambda_{10})$ (here we only consider the connected matrix elements in the chain (F1) and neglect other matrix elements), and finally obtain

$$\mathrm{L}\{\rho_{10}^{(3)}\} = \frac{-\mathrm{i}\,G_A \exp(\mathrm{i}\,\boldsymbol{k}_f \cdot \boldsymbol{r})(s+\Lambda_{30})}{s(s+\Lambda_{10})^2\{(s+\Lambda_{20})(s+\Lambda_{30}) + G_3^2\}}, \tag{1}$$

where $G_A = G_1G_2(G_2')^*$.

After the normalization of Eq.(1), we have

$$\mathrm{L}\{\rho_{10}^{(3)}\} = \frac{(s+\Lambda_{30})}{s(s+\Lambda_{10})^2\{(s+\Lambda_{20})(s+\Lambda_{30}) + G_3^2\}}. \tag{2}$$

The inverse-Laplace transformed solution of Eq.(2) can be expressed as

$$\rho_{10}^{(3)}(t) = A + \sum_{i=1}^{4} D_i\,|v|/\lambda_i + \sum_{i=1}^{4} D_i \exp(-\lambda_i t), \tag{3}$$

where $D_i$ and $\lambda_j$ are two tedious expressions, and $A = \Lambda_{30}/\Lambda_{10}^2(\Lambda_{20}\Lambda_{30} + G_3^2)$.

If the atomic thermal motion is taken into account, which is assumed to obey the Maxwell distribution $W(v) = (u\sqrt{\pi})^{-1}\exp(-v^2/u^2)$, where $u = \sqrt{2kT/m}$ with $m$ being the mass of an atom, $k$ is Boltzmann's constant, and $T$ is the absolute temperature, then the medium polarization in Eq.(4) is given

by

$$P(z) = N\mu_{10}\int_0^L \mathrm{d}z \int_{-\infty}^{\infty} \exp[-(v/u)^2[\Theta(v)\rho_{10}^{(3+)} + \Theta(-v)\rho_{10}^{(3-)}]\mathrm{d}v. \quad (4)$$

Here $L$ is the length of the thin cell, $\Theta(v)$ and $\Theta(-v)$ are Heaviside functions, $N$ is the density of atoms in the vapour, $\rho_{10}^{(3+)}$ and $\rho_{10}^{(3-)}$ are the density matrix elements for $v > 0$ and $v < 0$, respectively.[13] As usual in an ultra-thin cell, the initial conditions for the system are different for arriving ($v < 0$) and departing ($v > 0$) atoms. One has indeed [$\rho_{00}(L) = 1$, $\rho_{ij}(L) = 0$ $(i, j = 0, 1, 2, 3)$] for $v < 0$; and [$\rho_{00}(0) = 1$, $\rho_{ij}(0) = 0$ $(i, j = 0, 1, 2, 3)$] for $v > 0$.[3] Atoms experience inelastic collisions with the walls during which they lose optical excitation and all memory about the previous state, so it is justified to assume that the atoms will get de-excited with a collision with the wall, and are in the ground states at the instant they leave the wall after a collision. Thus, we use $t = z/v$ for $v > 0$ and $t = (z - L)/v$ for $v < 0$. Equation (4) changes the integration orders of $v$ and $z$, so one has $P(z) = N\mu_{10}\int_{-\infty}^{\infty} W(v)B_F(v)\mathrm{d}v$, where

$$B_F(v) = AL + D_i|v|/\lambda_i + D_i|v|\exp(L\lambda_i/|v|)/\lambda_i. \quad (5)$$

We assume

$$S_{F1} = \int_{-\infty}^{\infty} W(v)AL\mathrm{d}v,$$

$$S_{F2} = \int_{-\infty}^{\infty} W(v)(D_i|v|/\lambda_i)\mathrm{d}v,$$

$$S_{F3} = \int_{-\infty}^{\infty} W(v)(D_i|v|\exp(L\lambda_i/|v|)/\lambda_i)\mathrm{d}v,$$

$$S_F = S_{F1} + S_{F2} + S_{F3}.$$

The first term ("Doppler-broadened term") in Eq.(5) provides the usual steady-state Doppler-broadened spectra expected in confined cells.[13] Since Dicke-narrowing features are associated with transient effects as considered in both latter terms ("Dicke-narrowing terms"), it can be seen that the second term in Eq.(5) originates from the buildup of the atomic response to the excitation fields. It illustrates the integration of all possible interactions inside the medium, while the third term in Eq.(5) reflects the finiteness of the interaction time $L/v$, which is limited by the film thickness. When $L$ is long enough, $S_{F2}$ and $S_{F3}$ can be neglected (i.e. $S_F \approx S_{F1}$). Only polarization interference needs to be considered in this case.

The FWM signal intensity is also given by

$$I \propto |S_F|^2 = \left|\int_{-\infty}^{\infty} W(v)B_F(v)\mathrm{d}v\right|^2,$$

when $L$ is long enough, corresponding to the free space. So the nonlinear polarization $P$ to the FWM signal is given $P \propto \int_{-\infty}^{\infty}\mathrm{d}vW(v)F_F(v)$, where

$$F_F(v) = \Lambda_{30}/[\Lambda_{10}^2(\Lambda_{20}\Lambda_{30} + G_3^2)], \quad (6)$$

In particular, we can see that equation (6) is equal to the first term in Eq.(3). This means that the "Doppler-broadened term" $A$ in the thin cell is expected to be the same as the long cell term $F(v)$. So when $L$ is long enough, the FWM signal spectra in the long cell are similar to those in the case of a hot atom sample in free space.

When $L$ is long enough and $v = 0$, we will have the following equation corresponding to the case of a cold atom sample,

$$\rho_{10}^{(3)} = \frac{-\mathrm{i}\,G_A\exp(\mathrm{i}\,\boldsymbol{k}_f\cdot\boldsymbol{r})}{d_{10}^2\,(d_{20} + |G_3|^2/d_{30})}, \quad (7)$$

where $d_{10} = \Gamma_{10} + \mathrm{i}\,\Delta_1$, $d_{20} = \Gamma_{20} + \mathrm{i}(\Delta_1 + \Delta_2)$, $d_{30} = \Gamma_{30} + \mathrm{i}(\Delta_1 + \Delta_2 - \Delta_3)$.

We obtain the fifth-order matrix $\rho_{10}^{(5)}$ of SWM in the $|0\rangle - |1\rangle - |2\rangle - |3\rangle$ system, as shown in Fig.1(b). According to the SWM perturbation chain, we can obtain

$$\mathrm{L}\{\rho_{10}^{(5)}\} = \frac{\mathrm{i}\,G_s\exp(\mathrm{i}\,\boldsymbol{k}_s\boldsymbol{r})}{s(s+\Lambda_{10})^2(s+\Lambda_{20})^2(s+\Lambda_{30})}, \quad (8)$$

where $G_s = G_1G_2G_2^*G_3G_3^*$.

Similar to the procedure for FWM signal spectra, we can obtain the medium polarization $P = N\mu_{10}\int_{-\infty}^{\infty} W(v)B_S(v)\mathrm{d}v$, where $B_S(v) = AL + D_i|v|/\lambda_i + D_i|v|\exp(L\lambda_i/|v|)/\lambda_i$, and $A = 1/\Lambda_{10}^2\Lambda_{20}^2\Lambda_{30}$.

Similarly, we assume

$$S_{S1} = \int_{-\infty}^{\infty} W(v)AL\mathrm{d}v,$$

$$S_{S2} = \int_{-\infty}^{\infty} W(v)(D_i|v|/\lambda_i)\mathrm{d}v,$$

$$S_{S3} = \int_{-\infty}^{\infty} W(v)(D_i|v|\exp(L\lambda_i/|v|)/\lambda_i)\mathrm{d}v,$$

and

$$S_S = S_{S1} + S_{S2} + S_{S3}.$$

The SWM signal intensity is given by $I \propto |S_S|^2$. Obviously, when the cell length is large enough, we can

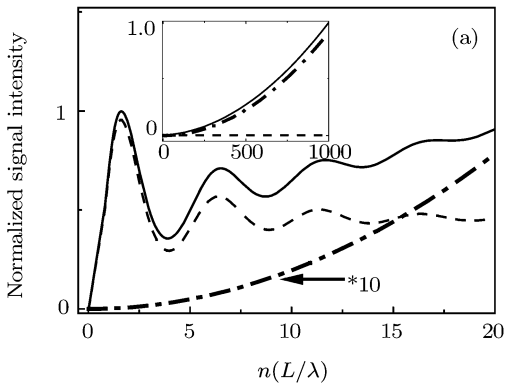
obtain $P \propto \int_{-\infty}^{\infty} \mathrm{d}v W(v) F(v)$ in the case of a hot atom, where $F_S(v) = \mathrm{i}/\Lambda_{10}^2 \Lambda_{20}^2 \Lambda_{30}$.

We have discussed the coexistence of FWM and SWM in the four-level confined system. It is well known that when the cell length is large enough, the sub-Doppler feature vanishes, and only a residual Doppler-broadened response is allowed. We have analysed the Doppler-broadened term in the thin cell, which is expected to be the same as the long cell term $F_S(v)$. From the expressions of FWM and SWM signal intensities, we can see that there exists polarization interference. To investigate the polarization interference, instead of calculating $\langle |S_F|^2 \rangle$ and $\langle |S_S|^2 \rangle$, we can sum up the signal intensity of each atom motion, i.e., $\int_{-\infty}^{+\infty} \mathrm{d}\nu W(v) \langle |B_S(v)|^2 \rangle$ without considering the inter-atomic polarization interference. In the next section, we will plot the normalized FWM and SWM spectra in ultra-thin, micrometre and long vapour cells, based on the analytic expressions above.

# 3. Numerical results and discussion

Figure 2(a) shows the SWM signal intensity spectra versus $n(L/\lambda)$. First, when $L$ is short (i.e. $L \leq 10\lambda$, corresponding to the thin cell), the SWM signal intensity varies with a $5\lambda$ period, the value of $|S_S|^2$ can be approximated to the value of $|S_{S2} + S_{S3}|^2$, and the "Doppler-broadened term" can be neglected. Second, there exists competition between Dicke-narrowing features and polarization interference in the micrometre cell. When $L$ increases, the contribution of polarization interference increases, while the effect of Dicke-narrowing features decreases. Finally, when $L$ is large enough (i.e., $L \geq 500\lambda$, corresponding to the long cell), the SWM signal intensity $|S_S|^2$ can be approximated to $|S_{S1}|^2$, i.e., the effect of Dicke-narrowing features can be neglected as shown in the inset in Fig.2(a).

To investigate how the oscillation behaviours are in the SWM signal intensity, we have Figs.2(b) and 2(c) that present the imaginary part $B_S''(v)$, and real part $B_S'(v)$ of $B_S$, respectively. Since the contribution of the "Doppler-broadened term" can be neglected, as compared to "Dicke-narrowing term", only the latter is considered in Fig.2(a). The real part $B_S'(v)$ shows a dispersive line shape, which leads to $\int_{-\infty}^{\infty} \mathrm{d}v W(v) B_S'(v) = 0$; therefore, only the imaginary part $B_S''(v)$ makes a contribution to the SWM signal. Since $B_S''(v)$ changes sign on the wings of both the $v < 0$ and $v > 0$ sides, destructive interference occurs between atoms, thereby suppressing the total polarization $P$. When $L = 3\lambda/2$, destructive interference is minimal, so the SWM signal intensity shows a maximal value, with periodic revivals at $L = (10k+3)\lambda/2$. When $L = 4\lambda$, destructive interference is maximal, so the SWM signal intensity is minimal. Therefore, the oscillation behaviour of the SWM signal intensity results from destructive interference. In addition, the imaginary parts of $B_S$ can be expressed by Euler transformation (the real part does not contribute to the signal): $AL + B[1-\cos(b\pi L/\lambda)] + C[1-\cos(c\pi L/\lambda)] + D[1-\cos(d\pi L/\lambda)]$, where $B$, $b$, $C$, $c$ and $D$, $d$ are coefficients of one-photon, two-photon and three-photon terms, respectively. As we know, for the absorption in a two-level system in the thin cell,[3] the second term corresponds to the one-photon term ("Dicke-narrowing term"). Thus, for the absorption spectrum, it shows the period $\lambda$, while the second, third and fourth terms correspond to the one-photon, two-photon and three-photon terms ("Dicke-narrowing term") respectively, causing the periodic behaviours of the SWM signal intensities and the drastic change in linewidths.



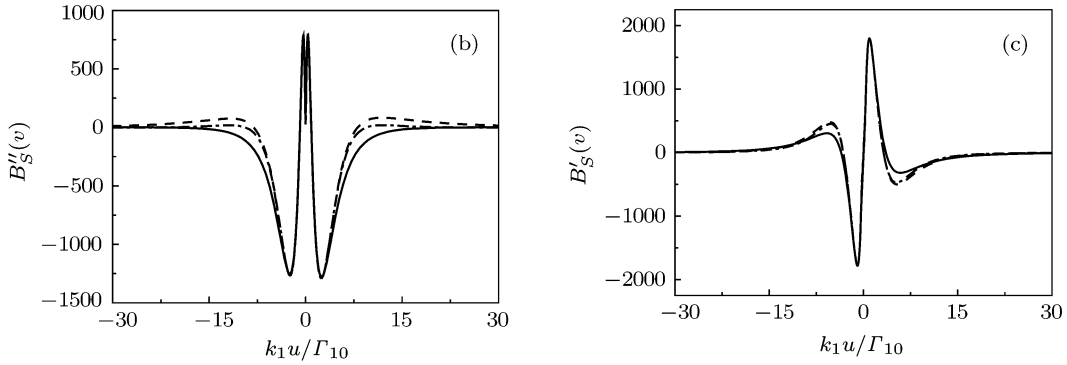



**Fig.2.** (a) SWM signal intensity versus $n(L/\lambda)$ for $|S_S|^2$ (solid curve), $|S_{S2}+S_{S3}|^2$ (dashed curves) and $|S_{S1}|^2$ (dot-dashed curves); (b) and (c) the imaginary and the real parts of $B_S$ when the "Doppler-broadened term" is neglected. $n = L/\lambda = 1.5$ (solid curve), 4 (dashed curve) and 6.5 (dot-dashed curve). Other parameters are $\Delta_1/\Gamma_{10} = 10$, $\Delta_2/\Gamma_{10} = -10$, $\Gamma_{10}/k_1u = \Gamma_{20}/k_1u = \Gamma_{30}/k_1u = 0.02$, $\xi_2 = 1.2$, $\xi_3 = 1.2$.

Figure 3 shows the line shape of SWM spectra dependent on cell length. In Fig.3, we can see that minimal values of the SWM spectra linewidth can be acquired at the cell length $L/\lambda = 4$ and 9. When $L/\lambda = 1.5$ and 6.5, the linewidths of the SWM spectra are broadened. There exists destructive interference in the ultra-thin cell; when $L/\lambda = 1.5$, destructive interference is minimum as shown in Fig.2(b), and the SWM signal linewidth is maximum. But destructive interference is maximum at $L/\lambda = 4$, and hence the SWM signal linewidth is minimum. So, at a larger destructive interference, the SWM signal shows a narrower spectrum, but this is opposite to the long cell case. When $L/\lambda = 20$, corresponding to the micrometre cell case, there exists competition between Dicke-narrowing features and polarization interference, the former acting in the line centre and the latter broadening the two shoulders of the SWM spectra, which increase monotonically as the cell length keeps increasing. When $L$ is long enough, corresponding to the long cell case, the polarization interference is dominant, the "Dicke-narrowing term" in $B_S$ can be

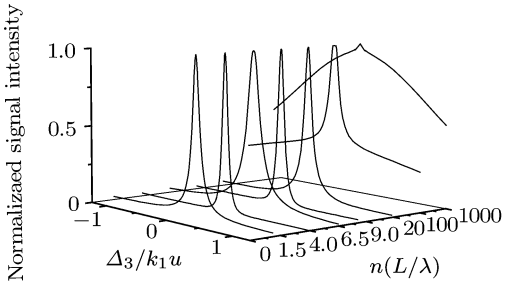



**Fig.3.** SWM spectra for $n = L/\lambda = 1.5$, 4, 6.5, 9, 20, 100, 1000, respectively, with $\Delta_1/\Gamma_{10} = 10$, $\Delta_2/\Gamma_{10} = -10$, $\Gamma_{10}/k_1u = \Gamma_{20}/k_1u = \Gamma_{30}/k_1u = 0.02$, $\xi_2 = 1.2$, $\xi_3 = 1.2$.

neglected, and only "Doppler-broadened terms" are considered, thereby the SWM spectra are broadened (e.g., $L/\lambda = 1000$).

We now investigate FWM spectra in the case of ultra-thin, micrometre and long cells. Figure 4(a) shows a comparison of the FWM spectra between the ultra-thin cell and the homogeneously broadened cases; both are in a general state and polarization interference is neglected. There is no destructive interference (see solid curve in Fig.4(c)) in the ultra-thin cell, therefore its FWM spectra are the same as those of the homogeneously broadened cases. As the intensity $G_3$ increases, a dip appears in the line centre, and then the spectrum splits into two separate peaks as shown in Fig.4(a). This is typical AT splitting. Moreover, the distance between the two peaks can be approximated as $\Delta_{G_3} \approx 2G_3$ under the condition $|G_3|^2 \gg \Gamma_{20}\Gamma_{30}$, where $\Delta_{G_3}$ is the separation induced by the dressing field $E_3$. On the other hand, as discussed in the previous section, when $L$ is long enough, due to the polarization interference, the linewidth of the FWM spectrum is much larger than that of the homogeneously broadened case in the absence of the dressing field (solid curve in Fig.4(b)). As $G_3$ increases, the linewidth of FWM spectra first becomes narrower, and then exhibits Doppler-free AT splitting again. This can be understood by studying the influence of the dressing field on $B''_F(v)$. We can see in Fig.4(d) that the application of the dressing field can suppress the polarization of atoms with $v = 0$, leading to a reduction of the destructive interference. Consequently, the linewidth of FWM spectra reduces, and Doppler-free AT splitting is exhibited.

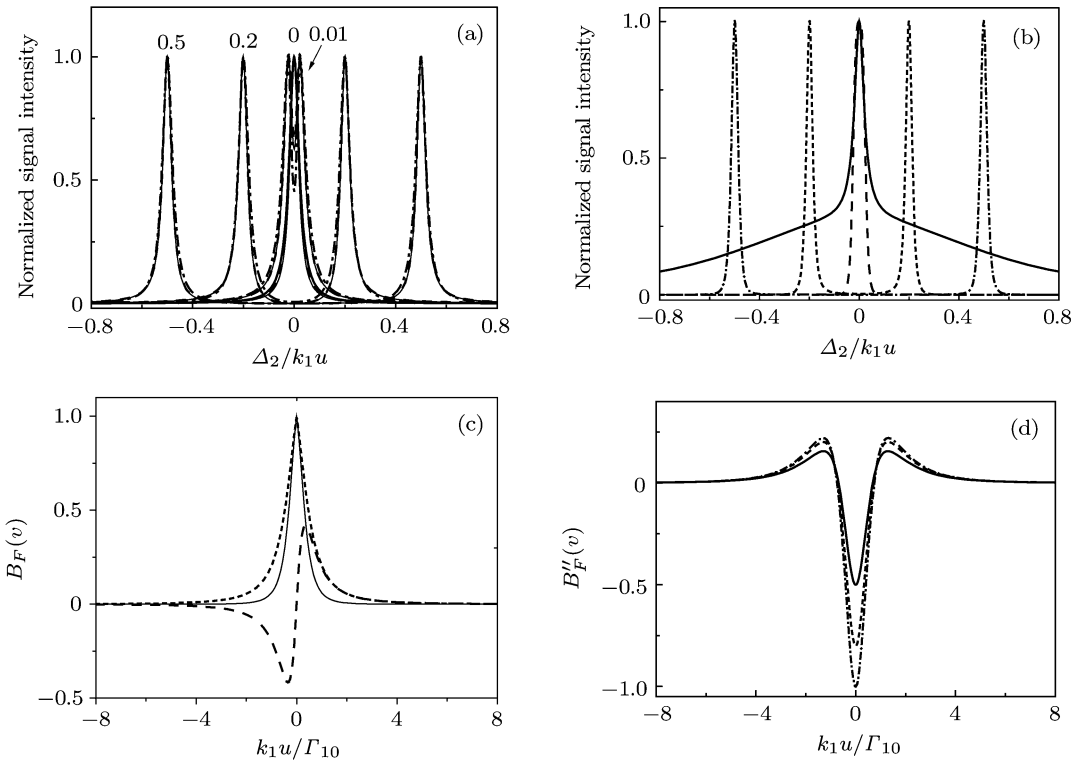



**Fig.4.** FWM spectra versus $\Delta_2$ for comparison: (a) the corresponding results of the homogeneously broadened cases (solid curves), $n = L/\lambda = 0.65$ (dashed curves) and when polarization interference is neglected (dot-dashed curves) ($G_3/k_1u$ is given near the curves). (b) FWM spectra versus $\Delta_2$ for $G_3/k_1u = 0$ (solid curve) $G_3/k_1u =$ 0.01 (dashed curve), $G_3/k_1u = 0.2$ (dotted curve), $G_3/k_1u = 0.5$ (dot-dashed curve), when $n = L/\lambda = 100$, $\Delta_1 = \Delta_2 = 0$. (c) Real part $B'_F(v)$ (solid curve), imaginary part $B''_F(v)$ (dashed curve) and absolute value $|B_F(v)|$ (dotted curve) when $n = L/\lambda$=100. (d) $B''(v)$ for $G_3/k_1u = 0$ (dot-dashed curve), $G_3/k_1u = 0.01$ (dashed curve), $G_3/k_1u = 0.02$ (solid curve) when the coupling field is exactly in resonance, when $\Delta_1 = \Delta_2 = 0$ and $n = L/\lambda = 100$. Other parameters are $\Gamma_{10}/k_1u = \Gamma_{20}/k_1u = \Gamma_{30}/k_1u = 0.02$, $\xi_2$= 0.6, $\xi_3$= 1.2.

Finally, we deal with the suppression or enhancement of the FWM signal intensity versus $\Delta_3$ in ultrathin, micrometre and long cells. The FWM intensity with no coupling field is normalized to 1 and an intensity above or below "1" means enhancement or suppression of the FWM signal. Firstly, at the exact two-photon resonance, we see that the FWM signal intensity is suppressed when the frequency of the dressing field is scanned across the resonance ($\Delta_3 = 0$) in the homogeneously broadened cases (dotted curve in Fig.5(f)). Specifically, when $L = 0.65\lambda$, the FWM spectra shows the line shape of suppression (Fig.5(a)) for there exists no destructive interference (Fig.4(c)). Secondly, when the cell length is large enough, corresponding to free space, figure 5(e) shows a sharp contrast with that of the homogeneously broadened cases. To study the anomalous behaviour, we neglect polarization interference when calculating $\int_{-\infty}^{\infty} \mathrm{d}vW(v)\,|F_F(v)|^2$; the results are shown by the solid curve in Fig.5(f), and are consistent with those of the homogeneously broadened cases, proving that the anomalous behaviour is caused by polarization interference. It can be understood that the dressing field can suppress the polarization of atoms with $v$=0, leading to a reduction of the degree of destructive interference (Fig.4(d)). As a result, the FWM signal intensity is enhanced. Finally, for the micrometre cell, there exists competition between the polarization interference and Dicke-narrowing features. When the cell length keeps increasing, the contribution of the polarization interference increases and the effect of Dicke-narrowing features decreases, which result in an increase in the FWM signal intensity, so the FWM signal intensity shows the change from suppression in the ultra-thin cell, to semi-suppression and semi-enhancement, and to enhancement, as shown in Figs.5(b)–5(d).

In a strong dressing field with a large two-photon

detuning, the FWM signal intensity can be hugely enhanced due to the polarization interference,[13] while the FWM signal intensity is enhanced for the three-photon ($|0\rangle \rightarrow |1\rangle \rightarrow |2\rangle \rightarrow |+\rangle$) resonance (Fig.1(d)).

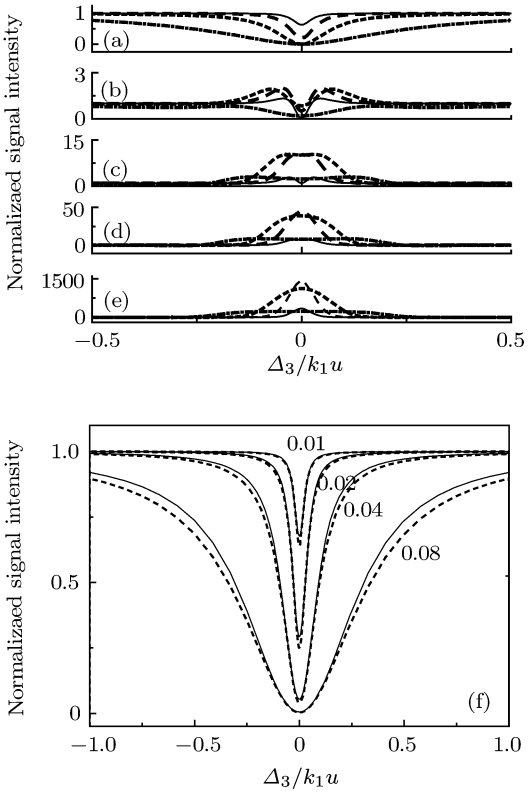



**Fig.5.** FWM signal intensity versus $\Delta_3$: (a) $L/\lambda = 0.65$, (b) $L/\lambda = 1.8$, (c) $L/\lambda = 5$, (d) $L/\lambda = 10$, (e) $L/\lambda = 100$. When $G_3/k_1u = 0.01$ (solid curves), $G_3/k_1u = 0.02$ (dashed curves), $G_3/k_1u = 0.04$ (short dashed curves), $G_3/k_1u = 0.08$ (dot-dashed curves). (f) Corresponding results when polarization is neglected with $\xi_2$= 0.6 (solid curves) and the homogeneously broadened cases (dotted curves) ($G_3/k_1u$ is given near the curves). Other parameters are $\Delta_1$=$\Delta_2 = 0$, $\Gamma_{10}/k_1u = \Gamma_{20}/k_1u = \Gamma_{30}/k_1u$ = 0.02, $\xi_2$= 0.6 and $\xi_3$= 1.2. The FWM signal intensity with no coupling field is normalized to 1.

# 4. Discussion and conclusion

We have investigated coexisting FWM and SWM in ultra-thin, micrometre and long cells in detail. The narrow spectra of the SWM signal results from Dicke-narrowing in the ultra-thin cell. The SWM signal spectrum is broadened due to the polarization interference in the long cell. There exists competition between Dicke-narrowing features and polarization in the micrometre cell, so the SWM signal spectrum shows a Lorentz line shape. Dicke-narrowing features act in the line centre and the polarization interference broadens the two shoulders of the SWM spectrum; the linewidths of the SWM signal spectra increase monotonically as the cell length keeps increasing. We have shown the oscillation behaviour that results from destructive interference in the ultra-thin cell. With a larger destructive interference, the SWM signal intensity shows a minimum. We have also investigated multi-wave mixing (MWM) signal intensities which are drastically changed due to the polarization interference in the long cell. In the micrometre cell, the dressing field can suppress the polarization interference, leads to the narrowing of the linewidth of FWM spectra, and then exhibits Doppler-free AT splitting. In addition, the FWM signal is suppressed when the frequency of the dressing field is scanned across the resonance ($\Delta_3 = 0$) in the ultra-thin cell. In contrast, the FWM signal is enhanced due to polarization interference. The FWM signal spectra show a change from suppression in the ultra-thin cell to semi-suppression and semi-enhancement, and to enhancement as the cell length increases.

In conclusion, we have investigated the coexistence of FWM and SWM in a confined four-level atomic system. The oscillation behaviour of the SWM signal intensity and linewidth is due to destructive interference. In the thin cell the narrow spectra can be used for high precision measurements and metrological standards. FWM and SWM processes in multi-level confined atomic systems can be utilized to help us to understand the QED mechanism and optimize the generated high-order multi-channel nonlinear optical signals, which have potential applications in high precision measurements and production of better nonlinear optoelectronic devices.

# References

[1] Dicke R H 1955 *Phys. Rev.* **99** 532

[2] Wu Y and Deng L 2004 *Phys. Rev. Lett.* **93** 143904
Wu Y 2003 *Phys. Rev.* A **67** 013811

[3] Dutier G, Saltiel S, Bloch D and Ducloy M 2003 *J. Opt. Soc. Am.* B **20** 793
Andreeva C, Cartaleva S and Petrov L, Saltiel S, Sarkisyan D, Varzhapetyan T, Bloch D and Ducloy M 2007 *Phys. Rev.* A **76** 013837

[4] Harris S E 1997 *Phys. Today* **50** (6) 36
Gea-Banacloche, Li J Y, Jin S and Xiao M 1995 *Phys. Rev.* A **51** 576

[5] Petrosyan D and Malakyan Y P 2000 *Phys. Rev.* A **61** 053820
Failache H, Lenci L, Lezama A, Bloch D and Ducloy M 2007 *Phys. Rev.* A **76** 053826

[6] Sarkisyan D, Varzhapetyan T, Sarkisyan A, Malakyan Y, Papoyan a, Lezama A, Bloch D and Ducloy M 2004 *Phys. Rev.* A **69** 065802
Sargsyan A. Sarkisyan D and Papoyan A 2006 *Phys. Rev.* A **73** 033803

[7] Ai B, D S Glassner and R J Knize 1994 *Phys. Rev.* A **50** 3345

[8] Hemmer P R, Katz D P, Donoghue J, Cronin-Golomb M, Shahriar, M S and Kumar P 1995 *Opt. Lett.* **20** 982
Li Y and Xiao M 1996 *Opt. Lett.* **21** 1064
Lu B, Burkett W H and Xiao M 1998 *Opt. Lett.* **23** 804

[9] Rostovtsev Y V, Sariyanni Z E and Scully M O 2006 *Phys. Rev. Lett.* **97** 113001
Braje D A, Balic V, Goda S, Yin G Y and Harris S E 2004 *Phys. Rev. Lett.* **93** 183601

[10] Kang H, Hernandez G and Zhu Y F 2004 *Phys. Rev. Lett.* **93** 073601

[11] Zhang Y P, Brown A W and Xiao M 2007 *Opt. Lett.* **32** 1120
Zhang Y P and Xiao M 2007 *Appl. Phys. Lett.* **90** 111104
Zhang Y P, Brown A W and Xiao M 2007 *Phys. Rev. Lett.* **99** 123603

[12] Li Y Y, Zhang G Z and Zhou Y 2006 *Chin. Phys.* **15** 985
Li Y Y, Bai J, Zhang G Z, Zhang Y P and Gan C L 2006 *Acta Phys. Sin.* **55** 6293 (in Chinese)

[13] Zuo Z C, Sun J, Liu X, Wu L A and Fu P M 2007 *Phys. Rev.* A **75** 023805